



ELSEVIER

Nuclear Instruments and Methods in Physics Research A 471 (2001) 41–54

**NUCLEAR
INSTRUMENTS
& METHODS
IN PHYSICS
RESEARCH**
Section A

www.elsevier.com/locate/nima

Micropattern gas detectors: the CMS MSGC project and gaseous pixel detector applications

R. Bellazzini^{a,b,*}, A. Brez^a, G. Gariano^a, L. Latronico^c, N. Lumb^a,
A. Moggi^a, S. Reale^a, G. Spandre^a, M.M. Massai^a, M.A. Spezziga^a, A. Toropin^{a,d},
E. Costa^e, P. Soffitta^e, D. Pacella^f

^a INFN-Pisa and University of Pisa, Via Livronese 5821A, I-56010 S. Piero a Grado, Pisa, Italy

^b CERN, CH-1211 Geneva 23, Switzerland

^c INFN-Genova and University of Genova, Genova, Italy

^d INR, Russian Academy of Sciences, Moscow, Russia

^e Istituto di Astrofisica Spaziale del CNR, Via Fosso del Cavaliere 100, I-00133 Rome, Italy

^f Associazione EURATOM-ENEA sulla Fusione, CR Frascati, I-00044 Frascati, Rome, Italy

Abstract

We report recent results from the development and testing of two types of micropattern gas detectors—micro-strip gas chambers and GEM-based devices with two types of pixel read-out. Thirty-two micro-strip gas chambers were tested in a high intensity hadron beam as a milestone for CERN's Compact Muon Solenoid (CMS) experiment. The detectors were operated with voltage settings corresponding to 98% hit detection efficiency at CMS for a total high intensity exposure period of 493 h. All of the requirements expected by the milestone—gain stability, number of lost strips, spark rate, etc.—were met, with wide margins. In a separate investigation, we have coupled PCB pixel read-out planes to GEM foils. In one case, 2 mm × 2 mm pixels were fanned out to individual discriminators and scalars to provide very fast (2 MHz/pixel) read-out; this system has been used as an imaging device to provide diagnostic information in fusion experiments. The second type of device used smaller pixels (200 μm squares) and a Flash-ADC read-out system to reconstruct individual photoelectron tracks. The angular distribution of the tracks allows the polarisation direction of polarised X-ray sources to be identified, with possible applications for future space experiments studying celestial X-ray emissions. © 2001 Elsevier Science B.V. All rights reserved.

1. Introduction

The Micro-Strip Gas Chamber (MSGC) [1–4] is a position sensitive proportional counter whose operational principle is analogous to that of the Multi-Wire Proportional Chamber (MWPC) [5]. Photolithographic techniques are used to build

metallic strips on a supporting substrate; these electrodes are spaced at least an order of magnitude more closely than is possible for an MWPC. The MSGC offers significant advantages in terms of spatial resolution and rate capability, thus filling the gap between cheap but rate-limited traditional gas detectors and solid-state devices, which have excellent performance but are rather expensive. MSGCs were intensively developed for the inner tracker of the CMS experiment at

*Corresponding author. Tel.: +39-050-880-286.

E-mail address: bellazzini@pi.infn.it (R. Bellazzini).

CERN's future LHC accelerator. In the first half of this paper we report the results of a large-scale test-beam evaluation performed in an environment very similar to that expected at CMS.

Despite their clear advantages, MSGCs are generally physically fragile devices (the substrate is usually a thin layer of glass) and rely on rather advanced technologies for their fabrication, making them still relatively expensive. A recently introduced class of detectors exploits the procedures normally used to construct multi-layer printed-circuit boards (PCBs). The feature size obtained by this technique is larger than that attainable with photolithography but the device is cheap and robust and available in large dimensions. Examples of detectors based on advanced PCB technology are the GEM [6], the Micro-Groove Detector [7] and the WELL detector [8]. Examples of major experiments in which GEMs are being used are the COMPASS experiment at CERN [9] and HERA-B at Desy [10]. In the latter experiment a GEM foil is used as a pre-amplifying stage prior to final charge amplification and collection by an MSGC. Indeed a very attractive feature of the GEM is that it allows the charge amplifying and collection structures to be completely decoupled, allowing a high degree of flexibility when choosing the geometry of the read-out electrodes. We have exploited this feature to provide GEMs with pixel read-out for two diverse applications—imaging of fusion plasmas and the determination of the polarisation degree of celestial X-ray sources.

2. Test of CMS prototype MSGCs in a high intensity hadron beam

2.1. Detector characteristics

The MSGCs used for the tests were based on a design which resulted from several years of research focused on optimising the detectors for CMS. High rate capability and resistance to sparking were particularly important considerations. The electrode material was gold, deposited on a 300 μm thick DESAG 263 glass substrate which had been coated with a 1 μm layer of slightly

conductive Pestov glass. The substrate area was 25 cm \times 10 cm. The anode width was 7 μm , the anode–cathode separation was 50 μm and the pitch was 200 μm . The ‘advanced passivation’ technique—covering of the cathode edges and ends of all electrodes with a layer of polyimide—was employed to suppress streamer formation in regions of very high electric field. The gas mixture was neon/DME, 40/60. Further details of the detector characteristics, and full explanations of the MSGC operating principle, may be found in Refs. [11,12].

2.2. Experimental procedures

Thirty-two large area MSGCs were tested in a 350 MeV pion beam at the Paul Scherrer Institute (PSI), Villigen, Switzerland. The particle rate was approximately 6 kHz/mm², distributed over the whole active area of the detectors; this rate was maintained for a total integrated time of 493 h. The environment to which the detectors were subjected (particle rate, probability of heavily ionising particle production, etc.) closely matched that expected for the MSGC layers foreseen at CMS; a detailed discussion of this point is given in Ref. [13]. The high intensity running period was divided into 3 phases: one week of ‘hardening’, during which previously undetected small lithographic defects were expected to ‘burn out’; three weeks of continuous high intensity running with limits imposed on the acceptable number of strips lost (the CMS ‘milestone’ period); one week in which voltage margins would be studied by raising the S/N above the working point values.

The PSI trial was essentially a survivability test, and three main parameters were continuously checked to monitor the condition of the detectors—the signal to noise ratio, the number of ‘dead’ strips since the beginning of high intensity irradiation and the spark rate of each chamber. In addition, track reconstruction allowed the efficiencies of the chambers to be evaluated.

Eight of the detectors were mounted with their strips at a small stereo angle to the vertical (all other detector strips being exactly vertical). This configuration allowed two-dimensional track reconstruction, enabling us to study the imaging capabilities of the system.

2.3. Results

The average signal to noise ratio of all of the detectors over the ‘milestone’ period (376 integrated hours of high intensity beam) is plotted in Fig. 1. The S/N corresponding to 98% hit detection efficiency at CMS (the ‘working point’ S/N) is 28 [12], lower horizontal line; all of the chambers were run at or above this value for the whole high intensity period. The overall average S/N value from Fig. 1 is 31, which was reached with an average cathode voltage of 515 V (drift field approximately 10 kV/cm) in the Ne/DME, 40/60 gas mixture. There is no evidence of any gain reduction due to ageing effects (the short-term variations in S/N visible in the plot are most likely due to changes in atmospheric pressure).

The stability of the detectors was also studied for S/N values significantly above the working point. While the S/N of eight reference chambers was kept at the usual value, the cathode voltages on the remaining 24 detectors were raised to give an average S/N of 39, see Fig. 2. The voltages on half of this group of 24 were later further raised; this process was continued until six chambers were

running at an S/N of 67 (2.4 times the working point value). The total duration of this study was approximately one week, and no degradation in chamber performance was observed.

The observed strip losses for the whole high intensity period (hardening, milestone and margins) are summarised in Fig. 3. Damaged strips were detected by comparing the noise of each strip with the start value; broken strips contribute a lower capacitance and hence have lower noise than an intact electrode. A total of 4 out of the 16,384 channels were lost during the hardening phase; 3 were broken in the 3-week milestone period; one further channel loss was detected during the margins study. The integrated high intensity times for these periods were 43, 376 and 74 h respectively. Extrapolating to 10 years’ running under LHC conditions, we calculate that the expected strip loss would be 0.5%, which is 20 times lower than the CMS milestone requirement.

The low rate of strip loss was largely due to the optimised design of the detectors (see Section 2.1), which ensured that the spark activity in the chambers was extremely low, Fig. 4. The plot

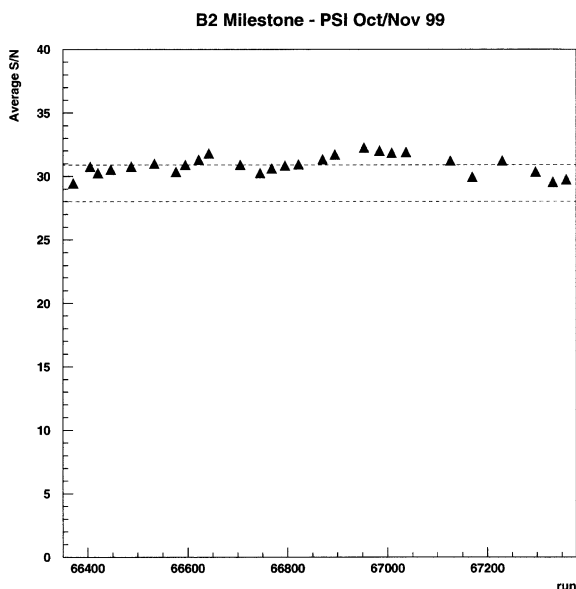


Fig. 1. Off-line S/N peak position averaged over all chambers for the milestone period.

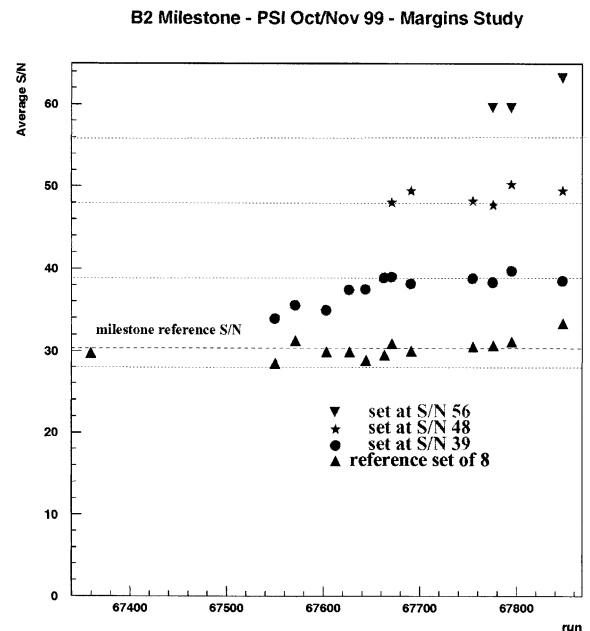


Fig. 2. Variation of average S/N with run number (margins period) for each of the different sets of detectors.

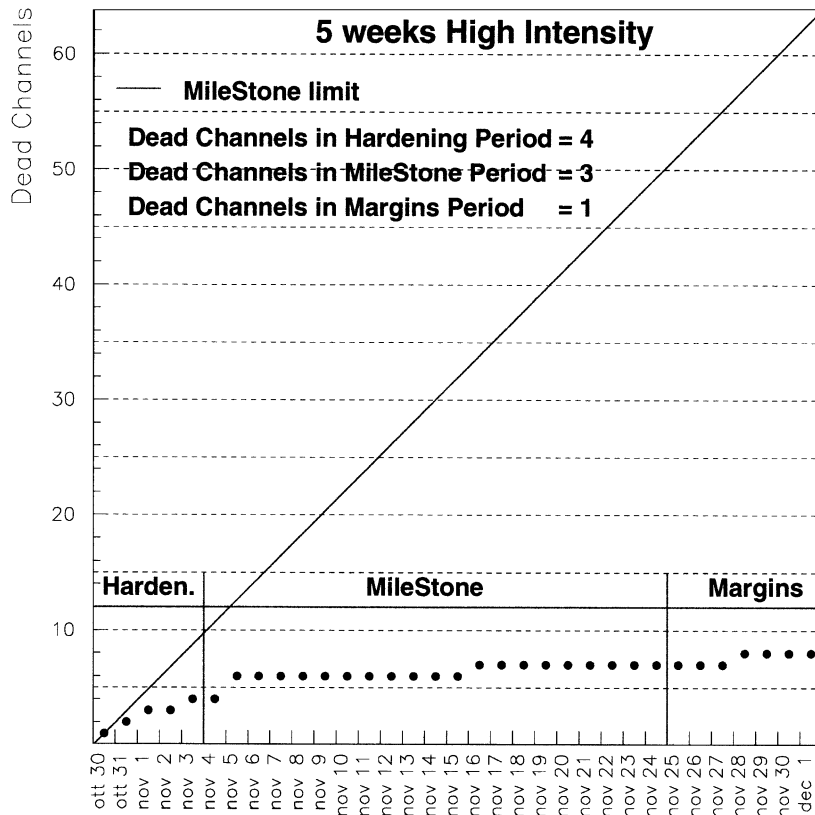


Fig. 3. Summary of all channel losses during the complete high intensity running period.

shows the spark rate as a function of time (run number). The chambers were divided into two boxes, with 16 chambers in each box. One of the boxes was closer to the beam pipe and the spark rate was higher in this box. The average values for both boxes are also shown in Fig. 4. The spark rate was low from the beginning (fewer than 1.5 sparks per chamber per day) and decreased with time in both boxes, reaching a minimum of 1 spark/chamber/day in the first box and an average value over the two crates of 0.7 sparks/chamber/day at the end of the milestone period. The rate in both crates increased only very slightly as the voltages were increased during the margins study but was always well below the initial rate.

A detailed analysis of the tracks through the chambers was performed and it was confirmed that the hit detection efficiency at CMS using the working point voltages would be above 98%

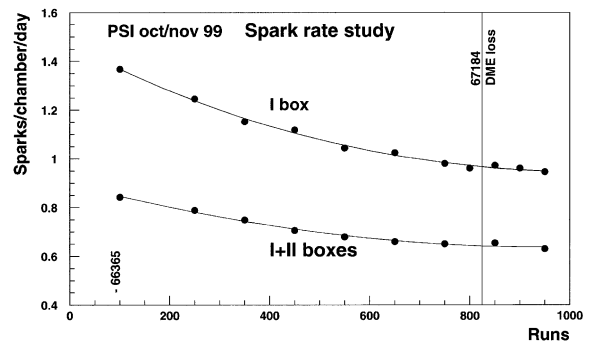


Fig. 4. Average spark rate as a function of run number for box 1 (closest to beam pipe, upper curve) and both boxes (lower curve).

(using these voltages at PSI the chambers were fully efficient, but due consideration had to be made for the increased ballistic deficit and noise of

the final CMS electronics). Taking advantage of the eight detectors with strips oriented at a small angle to the vertical ($\tan(\alpha)=0.1$), tracks could be reconstructed in two dimensions. Fig. 5 shows the image reconstructed after a thick brass mask with a pattern of holes drilled in it had been placed just in front of the first detector plate.

3. The gaseous pixel detector

The Gas Electron Multiplier (GEM) [6,14] consists of a layer of kapton, metallised on both sides, perforated by many thousands of tiny holes. By applying a potential difference across the foil, regions of very high electric field are generated in the holes. The introduction of a drift plane parallel

to the foil and a suitable gas environment results in a proportional counter capable of detecting ionising particles. True two-dimensional read-out may be achieved by measuring the very short currents (~ 20 ns) induced by extracting the avalanche electrons from the GEM holes and by transferring them to an array of metallised parts which will finally collect them. We have applied these ideas to provide detector solutions in two diverse areas of physics.

3.1. Real-time imaging of fusion plasmas

The TOKAMAK facility at INFN-Frascati (Rome) is used to study nuclear fusion. Plasmas are generated with a diameter of approximately 600 mm; the shape of the plasma is an important

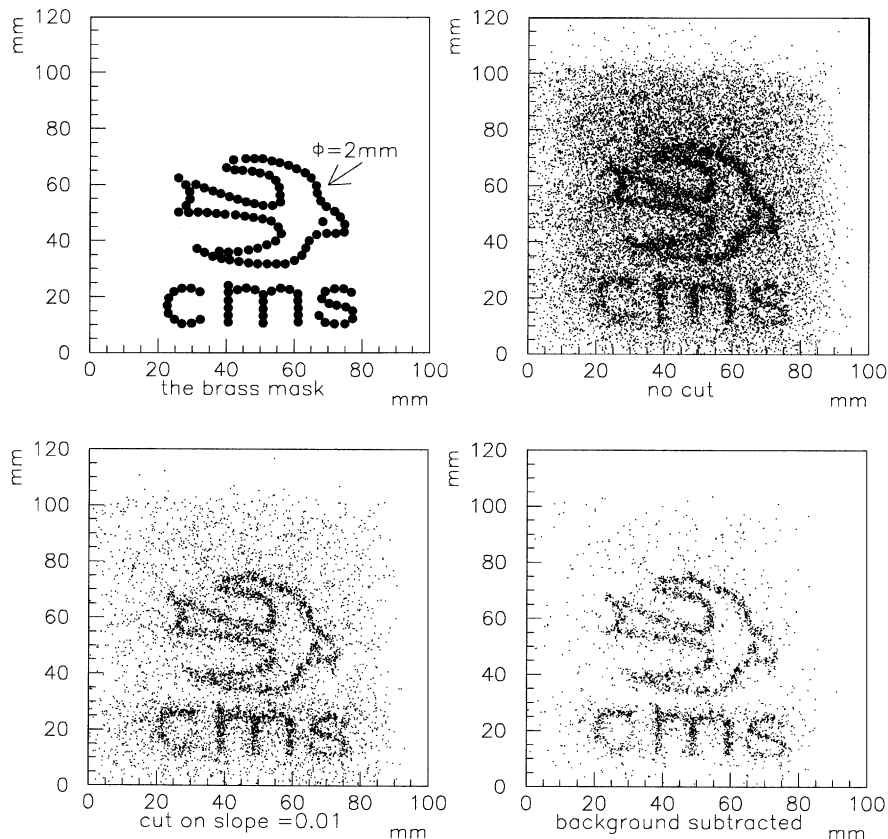


Fig. 5. The patterns of holes in the brass mask used for imaging studies was a swallow and the letters 'CMS'. The image reconstructed from the raw data is shown together with the improved image after application of a cut on the track angle and subtraction of the Gaussian background.

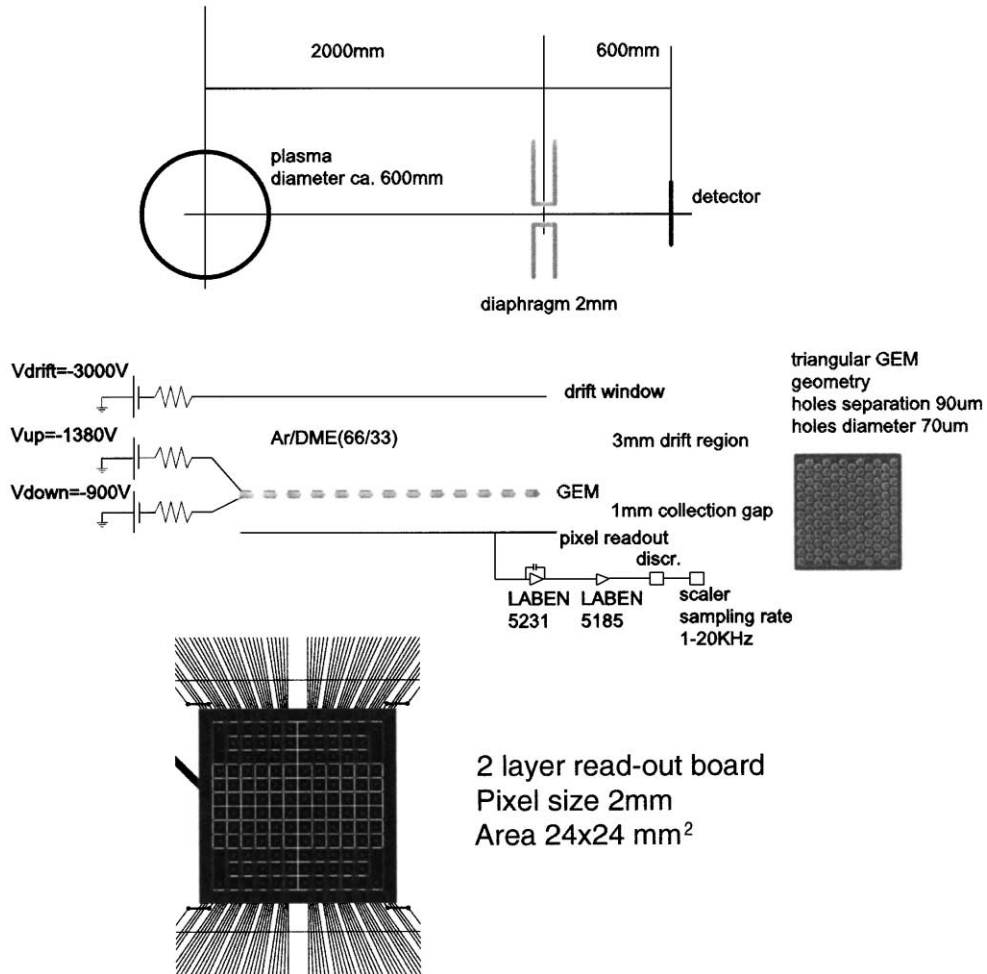


Fig. 6. A fast, two-dimensional X-ray imaging system for the real-time monitoring of fusion plasmas.

parameter which may be inferred from X-ray emissions. A fast, two-dimensional X-ray imaging system allows the plasma shape to be monitored in real time, see Fig. 6. A GEM mesh with a triangular hole pattern was used, with hole diameter of $70\ \mu\text{m}$ and hole separation of $90\ \mu\text{m}$. The gas mixture was argon/DME, 66/33 and the GEM and drift voltages were adjusted to achieve the required gain while maximising the GEM transparency (see Ref. [14] for a discussion of the GEM transparency).

The avalanche electrons produced in the GEM were collected by an array of 124 square pixels (side 2 mm) etched onto a PCB. Each pixel was

individually read out using a fast charge pre-amplifier (Laben 5231), an amplifier (Laben 5185), a low threshold discriminator and a latched scaler CAMAC (LeCroy 8590). The gain of the GEM (between 1000 and 2500 depending on the particular experimental circumstances) was high enough to provide signal well above the noise yet low enough to allow high counting rates (if the gain is too high space charge effects soon limit the rate capability of the detector).

The detector was first tested in the laboratory using a powerful (10 kW) X-ray tube operating at 20 kV. The discriminator thresholds were set above the noise but well below the value corre-

sponding to the low energy cut-off of 4 keV (determined by the absorption of the photons in air). The counting response of the detector was therefore largely independent of photon energy or small variations in gain between pixels. This response was checked for a range of tube currents and was found to be linear up to a photon rate of approximately 2 MHz/pixel. For higher fluxes, the scaler counts were non-linear with respect to the tube current due to the finite integration time of the electronics. The chamber response remained linear up to much higher photon rates; this was verified by measuring the signal current on the upper GEM layer, up to a maximum of 6 MHz/pixel.

Using the same laboratory set-up, and operating the X-ray tube at the top end of the linear counting region (2 MHz/pixel), the imaging capabilities of the detector were evaluated. First a lead plate with two pinholes with diameters 1 and 1.3 mm, separated by a distance of 8 mm, was inserted between the tube and the detector. As shown in Fig. 7, the holes were well resolved. The photons passing through the smaller pinhole were detected mainly on one pixel, whereas the counts corresponding to the larger hole were distributed over

four adjacent pixels. The total counts for each image were proportional to the respective areas of the pinholes.

In a second test, a small wrench was inserted into the X-ray beam, close to the detector—see Fig. 8. Again the data were acquired at a very high counting rate, approximately 2 MHz/pixel. Given the limited number of pixels, the shadow of the wrench is very well defined. The spatial resolution can be further improved by exploiting the fact that charge is shared between pixels and calculating the barycentre of the deposition. We emphasise the very high global acquisition rate—250 MHz over the whole detector—achievable using individual scalers for each pixel, allowing the image shown in Fig. 8 to be constructed within 1 ms.

Finally, the detector was tested using the high intensity X-ray emissions from fusion plasmas in the Frascati TOKAMAK. The X-ray energies are in the range 4–15 keV and the counting rate is typically 1 MHz/pixel, i.e. within the linear region of the detector. The image of the plasma was projected onto the detector plane by means of a 2 mm × 20 mm slit. Fig. 9 shows the results from two runs in which the counts from four adjacent

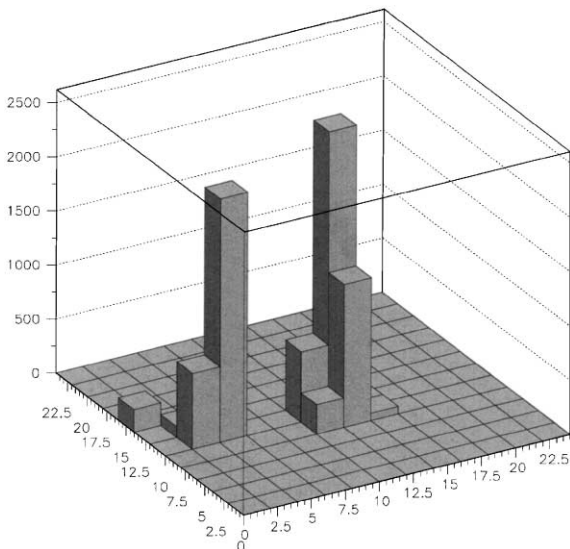


Fig. 7. Image formed by two pinholes, separation 8 mm, diameters 1 and 1.3 mm.

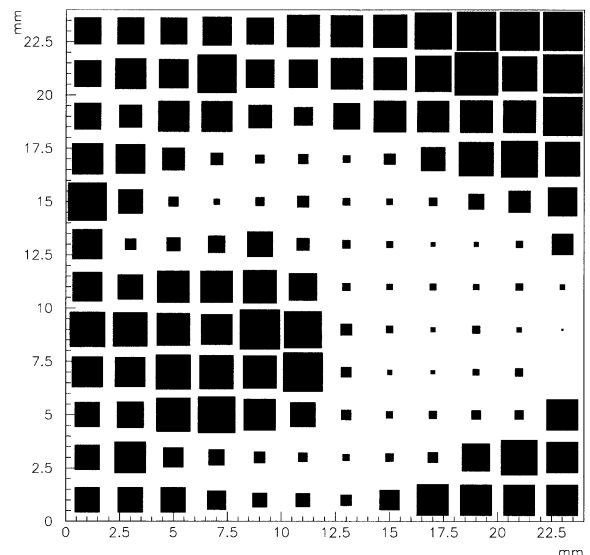


Fig. 8. Image of the head of a small wrench inserted into the X-ray beam. The area of each square is proportional to the recorded counts.

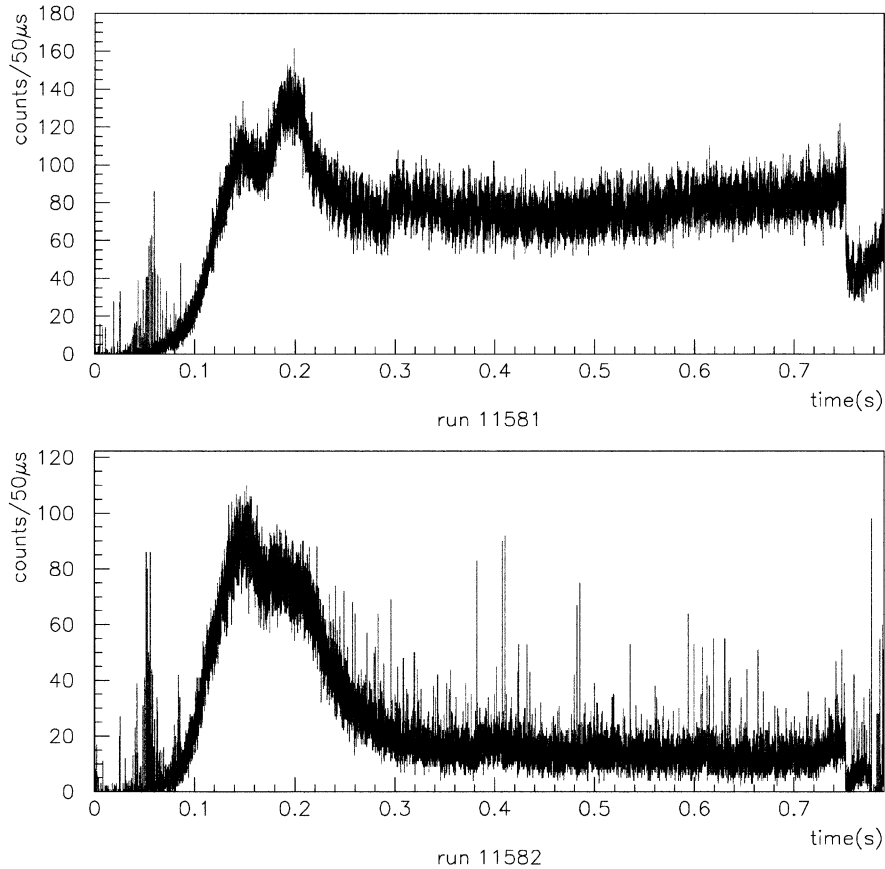


Fig. 9. Counts integrated over $50\mu\text{s}$ for four adjacent pixels centred on a fusion plasma in the Frascati TOKAMAK. Upper plot: plasma in steady state; lower plot: collapsed plasma.

pixels centred on the plasma were integrated over $50\mu\text{s}$ time slices. The upper plot shows a run during which the plasma was maintained for a relatively long period (maximum duration of plasma discharges is around 1.6 s for this TOKAMAK). The lower plot shows a case where the plasma collapsed. The information from the pixel detector was compared with the time evolution of the plasma temperature, see Fig. 10. Stimulation of the plasma by radiofrequency heating or the injection of hydrogen pellets was clearly recorded by both techniques.

In summary, a GEM has been coupled to a simple pixellised read-out board equipped with individual amplifiers and scalars. The resulting detector may be operated at very high counting

rates—up to 2 MHz/pixel (0.25 GHz globally)—making it an ideal choice as a diagnostic tool in the field of fusion plasma physics. The use of fast electronics could bring easily the overall acquisition rate in the GHz range.

3.2. X-ray polarimeter for space experiments

Many galactic and extra-galactic X-ray sources are polarised. The degree of polarisation is an important consideration when constructing models for the origins of these sources. The construction of a polarimeter to accurately measure this parameter is being considered for inclusion on board forthcoming space experiments. We propose a solution again based on a

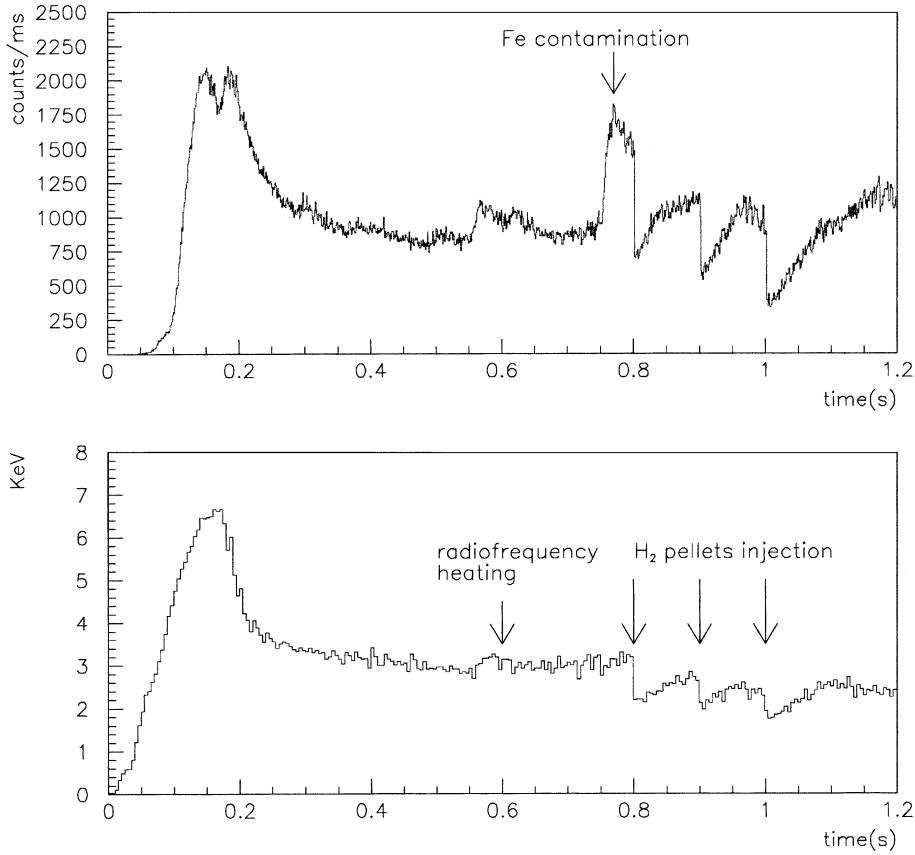


Fig. 10. Comparison of the time profiles from the pixel detector and from measurements of the plasma temperature.

GEM with pixel read-out, as shown in Fig. 11. The pixel size must be considerably smaller ($200\ \mu\text{m}$ squares) than for the device used to image fusion plasmas. The photon flux will be much lower, so a more conventional read-out system, in which each pixel is connected to a pre-amplifier and Flash-ADC channel, may be used. We again note the flexibility of using a gas amplification structure which is independent of the read-out. This allows the read-out to be tailored to the required application, without altering the overall design of the detector.

We have constructed a detector with 124 pixels built on an eight-layer PCB. The detector area ($2.4\ \text{mm} \times 2.4\ \text{mm}$) is very small but the high granularity allows the tracks of individual photo-

electrons emitted by each incident X-ray to be followed. For polarised sources, the directional distribution of the photoelectrons is not uniform but is governed by the equation

$$\frac{\delta\sigma}{\delta\Omega} = r_0^2 \frac{Z^5}{137^4} \left(\frac{mc^2}{h\nu}\right)^{7/2} \frac{4\sqrt{2} \sin^2(\theta)\cos^2(\phi)}{(1 - \beta \cos(\theta))^4}. \quad (1)$$

Here θ is the angle measured from the direction of the incoming photon and ϕ is measured with respect to the polarisation vector of the photon (refer Fig. 11). For a polarised X-ray beam incident perpendicular to the detector we expect the photoelectron tracks to lie preferentially in the

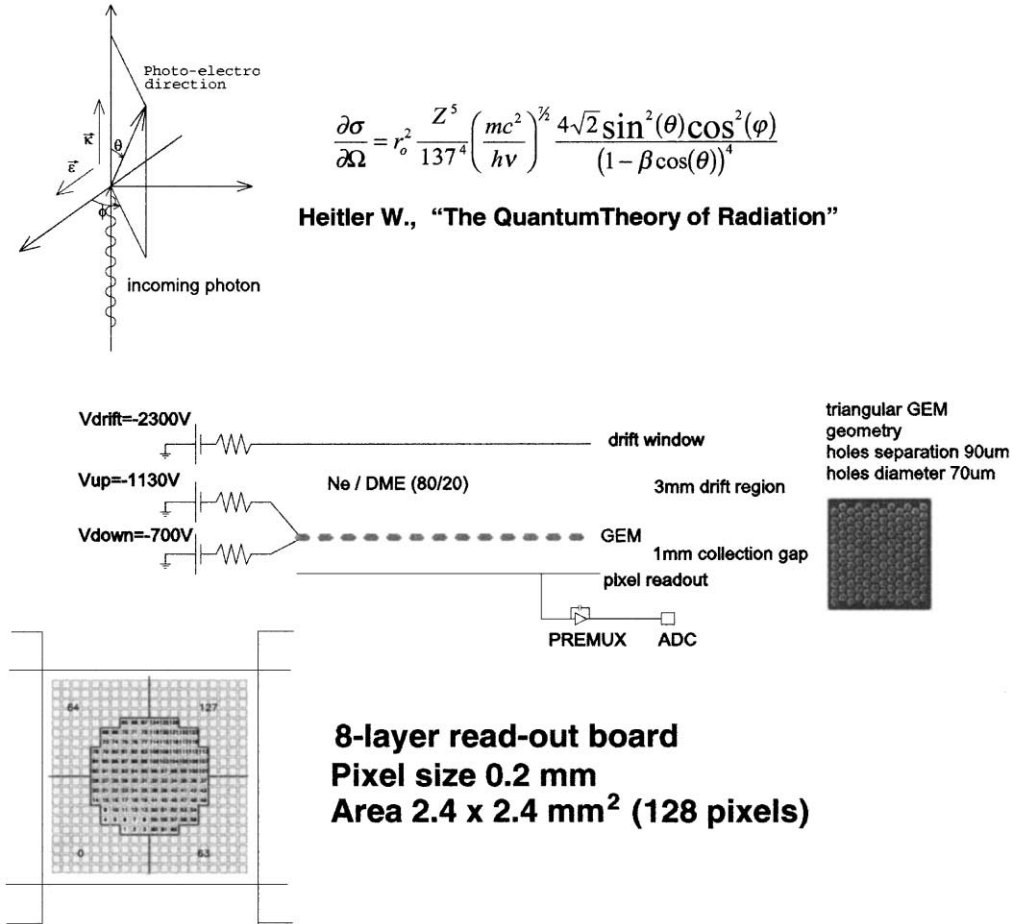


Fig. 11. A modified pixel read-out scheme allows the tracks of individual photoelectrons to be reconstructed. Analysis of the angular distribution of the tracks yields the direction of polarisation for polarised sources.

plane of the detector (from the $\sin^2(\theta)$ term), with a slight forward bending due to the theta dependence in the denominator. The projection of all tracks onto the detector plane is a squared cosine distribution peaked around the direction defined by the polarisation vector of the incident photon.

The detector was first tested by irradiating a very small ($50\ \mu\text{m}$) spot at the centre of the pixel pattern using a finely collimated, *unpolarised* beam from a X-ray tube (5.4 keV from a Cr target). The gas mixture was neon/DME, 80/20 and the electrode voltages were $V_{\text{drift}} = -2300\ \text{V}$, $V_{\text{GEM}}^{\text{up}} = -1130\ \text{V}$, $V_{\text{GEM}}^{\text{down}} = -700\ \text{V}$. The GEM

layer was identical in design to the one used for the fusion plasma studies. Four examples of clusters reconstructed by off-line software are shown in Fig. 12. It is expected, and indeed clearly observed in these examples, that most of the energy of the photoelectron is released at the end of its path. This fact is emphasised when a cumulative plot of the cluster barycentres is made, Fig. 13. Here we have applied a cut which rejects 'shapeless' clusters, selecting only those whose paths fall in a clearly defined direction. This direction can be characterised by an angle measured with respect to a chosen axis passing through the barycentre of the

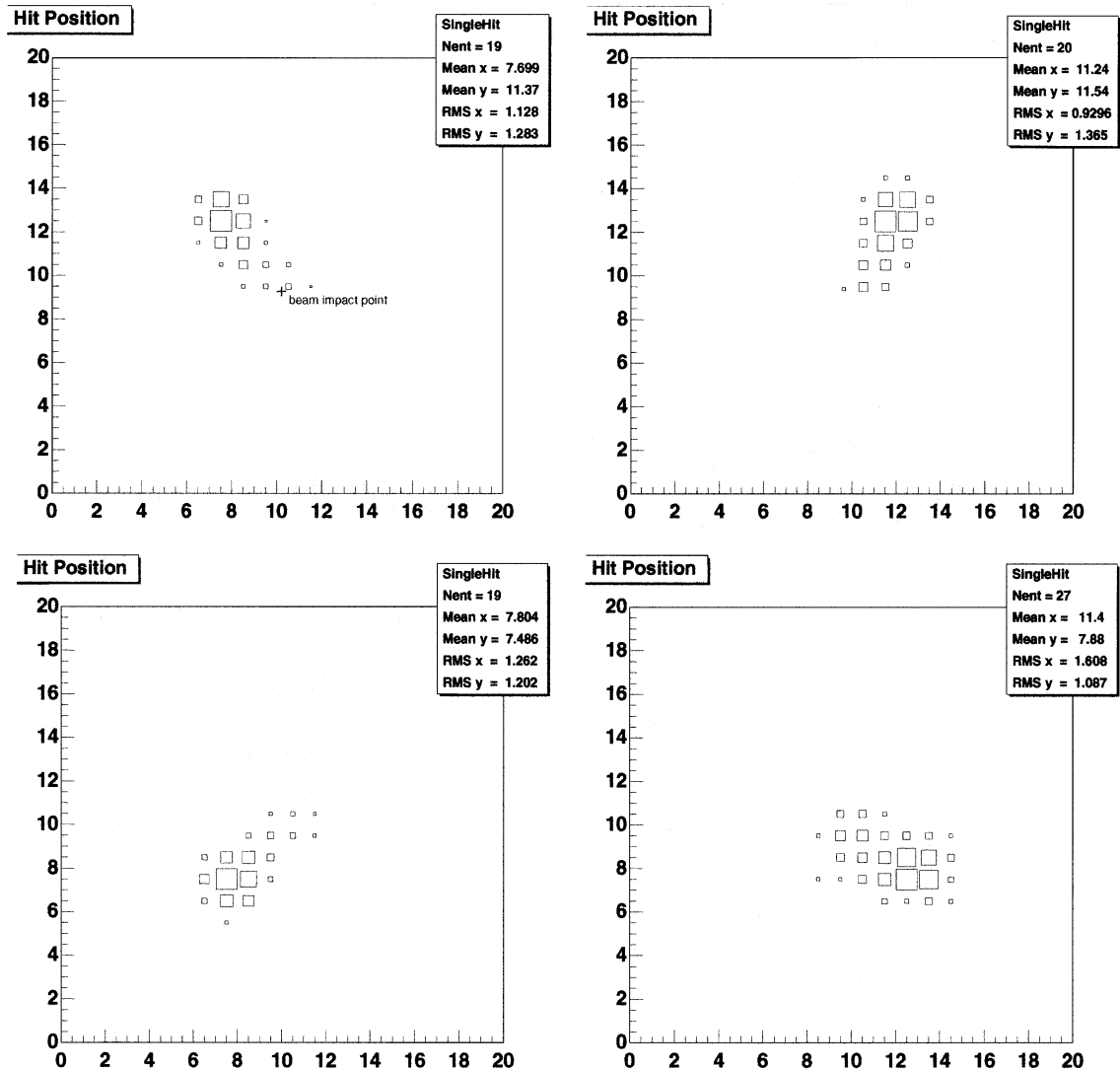


Fig. 12. Four tracks for photoelectrons released from a $50\ \mu\text{m}$ spot near the centre of the detector (unpolarised source). The beam spot corresponds approximately to the coordinate (10.0, 9.5) in the figure.

cluster. For the unpolarised source the angular distribution was, as expected, uniform (this is evident from the fact that Fig. 13 shows a circular distribution with no preferred angle). The cut on the cluster shape results in a ‘hole’ in the distribution, centred over the impact point of the X-ray beam. The fact that well over 50% of the events survived this cut convinced us that we were indeed able to image photoelectron tracks. This success encouraged us to study

polarised sources using the strategy described above.

Polarised X-rays were produced by introducing a lithium target into the beam emerging from the X-ray tube. A collimation system was used to select only photons Thomson scattered through 90° ; such photons should be fully polarised. This polarised beam was directed onto the pixel detector. For each photon releasing a photoelectron inside the detector, the direction of the

photoelectron was established; the angular distribution is plotted in Fig. 14 (right hand plot). There is a clear peak in the distribution (compare

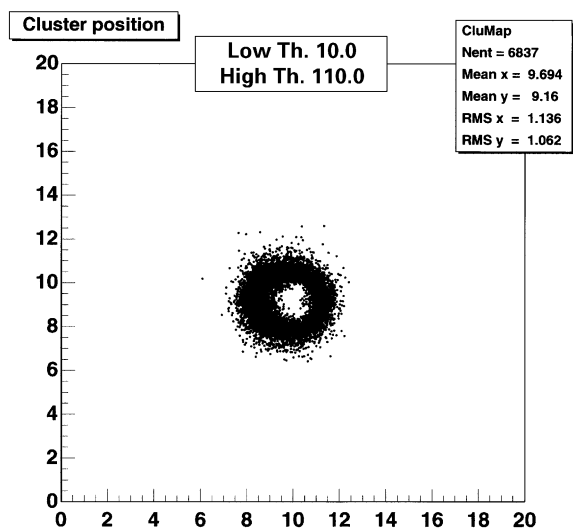


Fig. 13. Cumulative plot of barycentre position for several thousand clusters (unpolarised source).

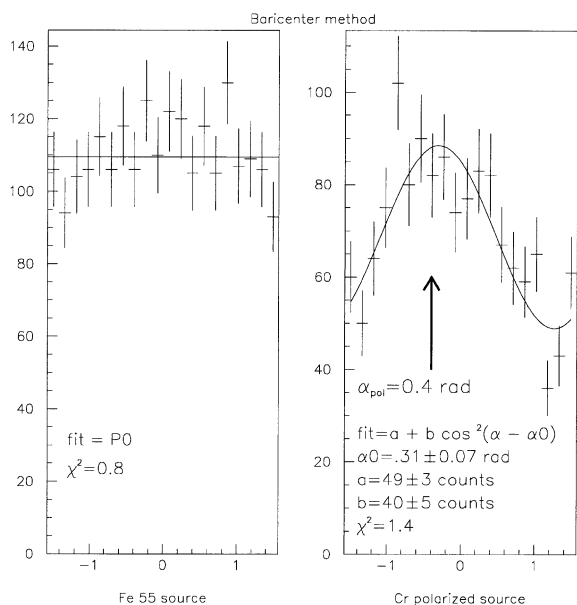


Fig. 14. Angular distribution of photoelectrons released in the detector for unpolarised ^{55}Fe source (left) and polarised source (right).

with results for an unpolarised ^{55}Fe source— Fig. 14, left hand plot). These data were taken with the detector oriented at an angle of approximately 0.4 rad with respect to the polarisation vector of the X-rays. Fitting a squared cosine to the data yields an offset angle of 0.31 ± 0.07 rad, in reasonable agreement with the measured detector orientation. The fitted data sit on top of a flat pedestal—an irreducible background due to the presence of clusters with no definite direction. Some of these clusters may be produced as a result of photoelectrons with a large component of their momenta outside of the plane of the detector (a second-order possibility allowed by Eq. (1)); the projections of such tracks onto the detector plane are less well reconstructed. A second contribution to the background may come from stochastic effects which cause early deviations in the direction of some photoelectrons, causing the angular information relating to the polarisation angle to be lost. We can define the modulation factor, M , where $M = (\text{Max} - \text{Min})/(\text{Max} + \text{Min})$; Min and Max are the minimum and maximum values of the fitted distribution. In terms of the fit parameters a and b in Fig. 14, $M = b/(2a + b)$. In our laboratory studies, we have achieved values for M between 30% and 50%. No real-life celestial X-ray source is fully polarised; in fact many are very weakly polarised. It is of interest to calculate the minimum percentage of polarisation that could be detected above the background with 99% confidence. This is strongly dependent upon the intensity of the source and modulation factor M . Knowing the limitations of the gaseous pixel detector in its present stage of development, and assuming the use of a standard optical system for imaging of the X-rays onto the detector, we can plot the minimum detectable polarisation (MDP) as a function of flux, see Fig. 15 (upper line). It can be seen that many interesting extra-galactic X-ray sources already lie within the reach of today's technology. The lower line on the same graph indicates what should be achievable through a reasonable research and development programme. Improvements that could be made to the detector in order to reach this goal include reducing the pixel pitch to $50\ \mu\text{m}$ and the use of a pressurised (4 atm) gas mixture.

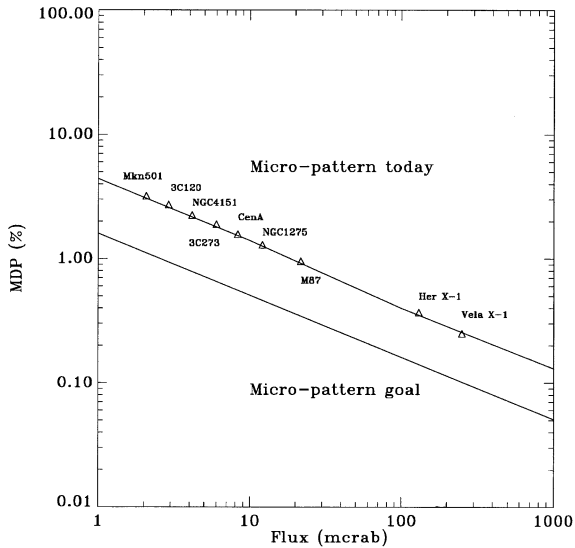


Fig. 15. Minimum detectable polarisation as a function of flux from the source for present-day gaseous pixel detector with standard X-ray optics (upper plot) and a reasonable research goal (lower plot). Flux is expressed in thousandths of the flux from the strong X-ray source in the Crab Nebula.

4. Conclusions

Micropattern gas detectors constitute a rapidly growing field of research which is delivering a class of device capable of filling the gap between solid-state detectors and more traditional gas detectors like the MWPC. The most mature and intensively researched device in this class is the MSGC, which has been used in many diverse applications both within and outside of particle physics. A more recent development has been the introduction of detectors based on advanced printed circuit board technology. The ‘artwork’ of these devices is generally coarser than that achievable using the microelectronics techniques with which MSGCs are produced; there are however distinct advantages in terms of cost and physical robustness. In the case of GEM, in which the process of avalanche multiplication is separated from the charge collection structures, there is the additional benefit of having great flexibility in read-out design.

We have developed and carefully optimised MSGCs to allow them to be used in the harsh

radiation environment presented by the CMS inner tracker. In a milestone test, 32 detectors were irradiated in a high intensity (6 kHz/mm^2) hadron beam for a total integrated period of 493 h. The signal-to-noise ratio of all the detectors was kept above the value corresponding to 98% hit detection efficiency at CMS for the duration of the test. The average observed spark rate was 0.7 sparks/chamber/day and the total strip loss extrapolated to 0.5% for 10 years’ running at LHC, 20 times lower than the milestone requirement. The chambers were tested for a one-week period at gains up to 2.4 times higher than the nominal value, without any significant increase in spark rate or strip loss. No evidence of ageing effects or unusual gain variations was observed throughout the evaluation period. The imaging capabilities of the detectors were explored by exploiting detectors with strips placed at a small stereo angle to the vertical.

A detector based on advanced PCB technology was developed for imaging fusion plasmas at the Frascati TOKAMAK facility. An array of 124 metallic pixels of side 2 mm was fanned out on a 2-layer PCB and used to read out charge amplified by a GEM layer. Signals from each pixel were amplified and passed through individual discriminators and scalars. This arrangement allowed very high acquisition rates (up to 2 MHz/pixel, 0.25 GHz globally). Following a series of successful laboratory tests, the detector was used to monitor X-ray emissions from fusion plasmas at Frascati. Comparison with existing techniques confirmed that the detector has the potential to become an important diagnostic tool in this field.

By simply replacing the pixel board with a different design, we have been able to contribute to the very different field of X-ray astrophysics. For this application, the much smaller ($200 \mu\text{m}$) pixels were fanned out on an 8-layer PCB. A Flash-ADC system was used in place of individual discriminators and scalars. This system was therefore much slower but allowed sophisticated clustering algorithms to reconstruct the tracks for individual photoelectrons released with the detector when exposed to an X-ray flux. By quantifying the direction of the tracks, the polarisation angle of low energy X-rays (5.4 keV) from a polarised

source could be measured. Such a system could be used on board a space experiment to investigate polarised celestial X-ray emissions.

Acknowledgements

The help and assistance of the PSI liaison staff and in particular of Dr. Dieter Renker is gratefully acknowledged. We would also like to thank Mr. L. Corucci and Mr. C. Salaris for their skilled technical support.

References

- [1] A. Oed, Nucl. Instr. and Meth. A 263 (1988) 351.
- [2] F. Angelini, et al., Nucl. Instr. and Meth. A 283 (1989) 755.
- [3] F. Angelini, et al., Nucl. Phys. 23A (1991) 254.
- [4] R. Bouclier, et al., Nucl. Instr. and Meth. A 323 (1992) 240.
- [5] G. Charpak, et al., Nucl. Instr. and Meth. 62 (1968) 235.
- [6] F. Sauli, Nucl. Instr. and Meth. A 386 (1997) 531.
- [7] R. Bellazzini, et al., Nucl. Instr. and Meth. A 424 (1999) 444.
- [8] R. Bellazzini, et al., Nucl. Instr. and Meth. A 423 (1999) 125.
- [9] L. Schmitt, The COMPASS Experiment, Proceedings of ICHEP98, Vancouver, 1998.
- [10] T. Hott, for the Hera-B Inner Tracker Collaboration, MSGC development for the inner tracker of Hera-B, presented at the fifth International Workshop on B-Physics at Hadron Machines, Los Angeles, 1997, Nucl. Instr. and Meth. A 408 (1998) 258.
- [11] CMS Technical Design Report, CERN/LHCC 98-6.
- [12] R. Bellazzini, et al., Nucl. Instr. and Meth. A 457 (2001) 22.
- [13] M. Huhtinen, Factors to scale highly ionising particle rates in MSGC irradiation tests to the LHC radiation environment, CMS Note 1997/073.
- [14] R. Bellazzini, et al. What is the real gain of a standard GEM? Nucl. Instr. and Meth. A 419 (1998) 429.